Electronic supplementary information

Survival of newly formed particles in haze conditions

Ruby Marten[1], Mao Xiao[1], Birte Rörup[2], Mingyi Wang[3], Weimeng Kong[4], Xu-cheng He[2], Dominik Stolzenburg[2], Joschka Pfeifer[5,6], Guillaume Marie[6], Dongyu S. Wang[1], Wiebke Scholz[7], Andrea Baccarini[1,8], Chuan Ping Lee[1], Antonio Amorim[9], Rima Baalbaki[2], David M. Bell[1], Barbara Bertozzi[10], Lucia Caudillo[6], Biwu Chu[2], Lubna Dada[1], Jonathan Duplissy[2], Henning Finkenzeller[11], Loïc Gonzalez Carracedo[12], Manuel Granzin[6], Armin Hansel[7], Martin Heinritzi[6], Victoria Hofbauer[3], Deniz Kemppainen[2], Andreas Kürten[6], Markus Lampimäki[2], Katrianne Lehtipalo[2,13], Vladimir Makhmutov[14], Hanna E. Manninen[5], Bernhard Mentler[7], Tuukka Petäjä[2], Maxim Philippov[14], Jiali Shen[2], Mario Simon[6], Yuri Stozhkov[14], António Tomé[15], Andrea Wagner[6], Yonghong Wang[2], Stefan K. Weber[5], Yusheng Wu[2], Marcel Zauner-Wieczorek[6], Joachim Curtius[6], Markku Kulmala[2], Ottmar Möhler[10], Rainer Volkamer[11], Paul M. Winkler[12], Douglas R. Worsnop, Josef Dommen[1], Richard C. Flagan[4], Jasper Kirkby[5,6], Neil M. Donahue[3], Houssni Lamkaddam[1,@], Urs Baltensperger[1], Imad El Haddad[1,@]

[1]Laboratory of Atmospheric Chemistry, Paul Scherrer Institute, 5232 Villigen, Switzerland.
[2]Institute for Atmospheric and Earth System Research (INAR)/ Physics, Faculty of Science, University of Helsinki, 00014 Helsinki, Finland.
[3]Center for Atmospheric Particle Studies, Carnegie Mellon University, 15213 Pittsburgh, PA, USA.
[4]California Institute of Technology, Division of Chemistry and Chemical Engineering 210-41, Pasadena, CA 91125, USA.
[5]CERN, CH-1211 Geneva, Switzerland.
[6]Institute for Atmospheric and Environmental Sciences, Goethe University Frankfurt, 60438 Frankfurt am Main, Germany.
[7]Institute of Ion Physics and Applied Physics, University of Innsbruck, 6020 Innsbruck, Austria
[8]Extreme Environments Research Laboratory (EERL), École Polytechnique Fédérale de Lausanne, Sion, CH.
[9]CENTRA and FCUL, University of Lisbon, 1749-016 Lisbon, Portugal.
[10]Institute of Meteorology and Climate Research, Karlsruhe Institute of Technology, 76021 Karlsruhe, Germany.
[11]Department of Chemistry & CIRES, University of Colorado Boulder, 215 UCB, Boulder, 80309, CO, USA.
[12]Faculty of Physics, University of Vienna, Boltzmanngasse 5, A-1090 Vienna, Austria.
[13]Finnish Meteorological Institute, Helsinki, Finland.
[14]Lebedev Physical Institute of the Russian Academy of Sciences, 119991, Moscow, Leninsky prospekt, 53, Russian Federation.
[15]IDL-Universidade da Beira Interior, 6201-001 Covilhã, Portugal.
[16]Aerodyne Research, 01821 Billerica, MA, USA.
[@]Corresponding authors e-mails: houssni.lamkaddam@psi.ch, imad.el-haddad@psi.ch.

Summary

This electronic supplementary information (ESI) document describes the CLOUD chamber and details of experimentation and instrumentation used at CLOUD, CERN. Details of the parameters calculated from CLOUD results (such as growth rates) and details of the kinetic model set up and equations used are also presented.

Methods

The CLOUD chamber at CERN

The CLOUD chamber is 26.1 cubic meters, is made of stainless steel, and the inside surface is electro-polished [1,2]. The chamber concentrations are kept homogeneous via turbulence created by two magnetically coupled stainless steel fans at the top and bottom of the chamber [3], with mixing times typically on the order of a few minutes. The dilution (ventilation) lifetime is 1.3 hours. Wall loss rates of gases and different sized particles are also well characterised [4]. Precursor gases are injected via a state-of-the-art gas system that allows us to control dilution and injection flows to control the gas concentrations with great accuracy. The trace gases are injected into the chamber along with dry air, formed by mixing 79% boil-off nitrogen and 21% boil-off oxygen (both Messer, 99.999%) and water is added from an evaporator using ultrapure water (18 MΩ cm, Millipore Corporation) in order to control the relative humidity. Note that in this study experiments were done without use of the 3.5 GeV/c secondary pion beam (π beam) from the CERN PS.

The experiments presented in this paper involved varying mixtures of gases capable of nucleation and growth; sulfuric acid, ammonia, dimethylamine, nitric acid, and HOMs generated from toluene and α-pinene. Experiments started when lights were turned on and condensable gases were formed by photolysis (and further reactions). The various lights used in these experiments resulted in a homogeneous illumination of the chamber. These different sources were: three UV sources including four 200 W Hamamatsu Hg-Xe lamps (UVH), a 170 W quartz-clad high intensity Hg lamp (saber, LS1), and a 4 W KrF 248 nm excimer UV laser (UVX); further, UVA was generated at 385 nm by a 400 W UVA LED saber (LS3). LS1, UVH, and UVX were used to photolyse ozone, and LS3 was used to photolyse HONO, both in order to generate OH radicals. After each experiment, the particles and condensable gases were cleaned from the chamber by increasing the fan speed and thus the loss rates of particles, and gas concentrations were set up for the subsequent experiment.

The high condensation sink runs were extremely challenging to perform. For example, in instances where the condensation sink was decreasing over time, the gas phase NH_3 was constantly increasing, although the injection rate was constant. The large amount of HNO_3 generated in building up the condensation sink was also the cause of depletion of reagent ions in the Br^- CIMS, and so the HNO_3 was modelled for certain experiments (see modelling nitric acid).

Instrumentation

To measure gas-phase nitric acid, a Br^- chemical ionisation atmospheric pressure interface time of flight mass spectrometer (CI-API-TOF-MS) was deployed in the CLOUD chamber at CERN. We used a commercially available inlet from Airmodus for the mass spectrometer, which is optimised for minimum wall loss. The details of measurements can be found in the Methods section of Wang *et al*. (2020). During some experiments, the Br^- ion was depleted in the Br- CIMS due to high levels of HNO_3, and so HNO_3 was modelled from other time-series (see modelling nitric acid).

H_2SO_4 and HOMs were also measured by a CI-API-TOF-MS but with nitrate reagent ions. There were two NO_3^- CIMS present, one was equipped with an inlet from Airmodus, and the other used a home-made inlet and corona discharge for ion generation[5]. Both instruments were equipped with an electrostatic filter so as not to measure naturally formed ions from the CLOUD chamber. The detection limit of the condensable gases measured by the NO_3^- CIMS was approximately 5 x 10^4 cm^{-3}. Calibration techniques for H_2SO_4 and HOMs have been described previously [6,7].

Volatile organic compounds (VOCs) were measured by two different custom built proton transfer reaction time of flight mass spectrometers, a selective reagent ionization time of flight mass spectrometer (SRI-ToF-MS) described in Canaval *et al.* (2019)[8] and the PTR3-ToF-MS described in Breitenlechner *et al.* (2017)[9]. Both instruments used H_3O^+ ions to charge compounds of the sample gas. Humidity dependent calibrations of toluene were performed by directly measuring a gas standard (Apel Riemer Environmental Inc) at specific conditions of the respective experiments. These instruments were also used to analyze the cleanliness of the chamber in between experiments.

Ammonia and DMA were measured by a water cluster CI-API-TOF-MS, this instrument is described in detail in Pfeifer *et al*. (2020)[10]. The instrument introduced a newly designed cross-flow ion source. The authors report the limit of detection of ammonia to be ~ 0.5 pptv and predict the detection limit of DMA to be lower.

A suite of instruments covering different size ranges measured the particle number and size distribution between 1.5 nm and 487 nm. Starting with the smallest size, the instruments used were: a nano condensation nucleus counter (nCNC) [11]; a differential mobility analyser train (DMA-Train) [12]; a nano-scanning electrical mobility spectrometer (nSEMS) [13]; a nano-scanning mobility particle sizer (nano-SMPS); and a long SMPS.

The A11 nano Condensation Nucleus Counter is composed of a particle size magnifier (PSM) connected in series with a condensation particle counter (CPC). The PSM is an aerosol pre-conditioner that uses diethylene glycol (DEG) to grow aerosol particles to a size that is easily detected by the CPC. The saturator flow rate inside the PSM can be adjusted so aerosol particles of different sizes are activated. During CLOUD13, the PSM saturator flow was set to scanning, meaning it measured the particle size distribution between 1.5 and 2.5 nm [14,15].

The DMA train is built up of 6 different DMAs in parallel, measuring the range 1.8 - 4.3 nm each with different fixed voltages, to allow different size ranges, and the particles are counted by either a PSM or CPC depending on the size [12]; Stolzenburg *et al*. (2017) describe the instrument in detail.

The nSEMS is a newly developed instrument that operates in the range of 1.5 – 25 nm. For classification of particle size, the nSEMS uses a radial opposed migration ion and aerosol classifier (ROMIAC), which is capable of measuring particle diameters down to the nanometer level with less degradation and less sensitivity to diffusional resolution degradation than the DMAs. A full description of the instrument can be found in Kong *et al*. (2021)[13].

The nano and long SMPS are commercially available instruments and have been fully characterised and described in previous studies [16–18]. Together, the nano-SMPS and long-SMPS scan range spanned from 4 to 487 nm. Particles larger than 487 nm were formed during runs with high condensation

sinks. For these experiments, a multi-peak fitting routine was applied to deconvolve the observable size distribution into component modes, which were assumed to be lognormal in shape. The fitting results were then used to estimate the particle size distribution from 487 nm to 1036 nm. This was necessary for us to better calculate the condensation sinks and *J* rates, since the existence of larger particles will influence these parameters.

Ozone (O_3, Thermo Environmental Instruments, TEI 49C), sulfur dioxide (SO_2 Thermo Fischer Scientific Inc. 42i-TLE), and nitric oxide (NO, ECO Physics, CLD 780TR) were measured by gas monitors. Nitrogen dioxide was also measured but by a cavity attenuated phase shift NO_2 monitor (CAPS NO_2, Aerodyne Research Inc.). A custom-made cavity-enhanced differential optical absorption spectrometry instrument (CE-DOAS) was also used to measure NO_2 and HONO. Relative humidity of the chamber was measured by two instruments, dew point mirrors (EdgeTech) and an in situ-TDL-Hygrometer (KIT, CERN). Temperature was measured by mid-plane internal PT100 temperature sensors placed at 5 different distances from the chamber wall. The sensor that was closest to the midpoint of the chamber, 1.2 m from the wall, was used as the chamber's reference temperature.

Growth rates

Growth rates were calculated using the 50 % appearance time method [19]. This method works best in chamber or flow tube experiments, as it relies on the identification of a growing particle distribution easily differentiated from other particles. Since the CLOUD chamber is cleaned before each experiment, and new particles are nucleated from gases rather than injected, it is easy to differentiate the growing particles. This was more difficult in the case of the high condensation sink runs, as there were many pre-existing particles of different sizes, and thus the reason why growth rates are not reported for these runs. The model was set up to give output of different size bin concentrations at every time step (0.1 s) and so growth rates could be calculated in the same way as experimental data, where the sizing instrument output also gives size-distributed particle concentrations. Each size bin concentration over time is fit to the following function using a least-squares solver:

$$S_{d_p}(t) = \frac{a - b}{1 + (t/t_{app})^d} + b \qquad \text{(S.1)}$$

Size and time dependent growth rates calculated using the INSIDE method were presented in Figure 2.[20] This method is based on the adapted, size-integrated GDE, where the growth rate is solved for using experimental inputs for other variables. Full details of this method can be found in Pichelstorfer *et al*. (2018). [20] GDE-based GR methods might suffer from statistical fluctuations in the size-distribution measurement that may cause significant error. However, Ozon *et al.* (2021) [21] showed that for well-controlled chamber experiments, the INSIDE method agrees well with a fixed interval Kalman smoother which estimates the GR error for similar experiments to those in Figure 2a-e) to be roughly 1 nm hr^{-1}, or at maximum 50% for more dynamic situations such as in Figure 2f-j).

Where S_{dp} is the signal or concentration of a particular diameter (d_p) bin, *a* and *b* are the background and plateau concentrations respectively, *d* is a free parameter which relates to the steepness of the sigmoidal increasing curve, and t_{app} is the 50 % appearance time, which is equal to the time at which 50% of the concentration (in between background and plateau) has been reached. The appearance time for each bin is then plotted against the particle diameter and a linear fit is made to present

growth rates in nm hr^{-1}. For a full description see the Supporting Information of Stolzenburg *et al*. (2018)[19].

Formation rates

Formation rates were determined using the balance equation between the particle sources and sinks as per Dada et al. (2020)[22] shown in equation (S.2):

$$J_x = \frac{dN_{\geq x}}{dt} + S_{dil} + S_{wall} + S_{coag} \quad \text{(S.2)}$$

Where the units of J are (particles) cm^{-3} s^{-1} and S_{dil}, S_{wall}, and S_{coag} are terms for dilution loss, wall loss, and coagulation loss, respectively.

Formation rates of particles of diameter 2.5 nm were reported as a 2.5 nm particle is thermodynamically stable and larger than the critical radius [23]. 2.5 nm particles are also commonly measured in ambient campaigns and thus it is valuable for comparison. The total number concentration of particles with diameters 2.5 nm and above was measured using the nCNC.

Activation diameter

During the CLOUD experiments, when there was an activation event, the particle size bins just above the activation diameter tended to have low concentrations, due to fast growth after activation (faster than the time resolution of the instrument). The activation diameter was therefore determined by identifying the first time step where a bimodal distribution occurred, and the largest size bin of the smaller mode, where the concentration dropped, was identified as the activation diameter. For further information on this technique see the supporting information of Wang *et al*. (2020)[24].

Modelling ammonium nitrate

The flux of ammonia and nitric acid to a certain size particle is calculated using the following equation.

$$\phi_{i,p} = N_p^s \pi d_p^2 \underbrace{\left(\frac{E_{i,p}^{\mu} \varepsilon_{i,p} e_{i,p} \alpha_{i,p} \bar{s}_i B_{i,p}}{4}\right)}_{\text{Collision speed: } s_{I,p}^{\perp}} \underbrace{\left[c_i^v - a_{i,p}^s K_{i,p} c_i^o\right]}_{\text{Driving force: } F_{i,p}^{v,s}} \quad \text{(S.3)}$$

Area: A_p^s

Flux per unit surface area: $\varphi_{i,p}^{v,s}$

$$\bar{s}_i = \sqrt{\frac{8 k_b T}{\pi m_i}} \quad \text{(S.4)}$$

The subscript *i* denotes the gas species, i.e. NH_3 or HNO_3 (depending on which is limiting), and the subscript *p* refers to the particle size. Where N_p^s is the particle number and d_p is the diameter. The collision speed is derived from the average molecular speed (Equation (S.4)), and includes terms reflecting Van der Waals interactions between the vapour and particle (charge - dipole, dipole -

induced dipole, and induced dipole - induced dipole), $E_{i,p}^{\mu} = E^{\mu}(H_{i,p})$ where $H_{i,p}$ is the Hamaker constant in Joules; the non-zero size of the vapour, $\varepsilon_{i,p} = \left(d_i^2 + d_p^2\right)/d_p^2$; and the non-infinite mass of small clusters, $e_{i,p} = \sqrt{(m_i + m_p)/m_p}$. A term for gas-phase diffusion limitations is $B_{i,p} \simeq 1$ for large Knudsen numbers. The mass accommodation coefficient, $\alpha_{i,p}$, can also be included, this was assumed to be 1 for these calculations. The driving force depends on vapour concentration, c_i^v, and saturation concentration, c_i^o, as well as the activity in the solid phase and the kelvin term. Since the Hamaker constant for ammonia is 0, the enhancement from Van der Waals interaction is only relevant in acid-limiting conditions, and has the greatest effect at lower sized particles. This enhancement was not included in the thermodynamic model for this paper, but it may explain some of the difficulty in duplicating the experiment in Figure 2 Run 2, since the enhancement of growth at small sizes would have the small particles grow faster than the large particles in the CS.

We simplify the flux per unit surface area calculation to

$$\varphi_{i,p}^{v,s} = s_{i,p}^{\perp}\, c_i^v\, \gamma_{i,p} \tag{S.5}$$

$$\gamma_{i,p} = \left[1 - \frac{a_{i,p}^s}{a_i^v} K_{i,p}\right] \tag{S.6}$$

where $\gamma_{i,p}$ is defined as the uptake coefficient and can be defined in terms of the saturation ratio of the gas, where the saturation ratio is equal to the activity in the vapour phase divided by the activity in the solid phase times the kelvin term to account for the curvature of the surface of a particle.

$$\gamma_{i,p} = \left(1 - \frac{1}{S_{i,p}}\right) = \frac{S_{i,p} - 1}{S_{i,p}} = \frac{S_{i,p}^{XS}}{S_{i,p}} \tag{S.7}$$

$$S_{i,p} = \frac{a_i^v}{a_{i,p}^s K_{i,p}} \tag{S.8}$$

We can consider the flux as equal due to the 1:1 stoichiometry of condensation of ammonium nitrate, and thus we define a collision ratio, r^v_{AB}, which is the concentration ratio scaled by the collision speed of each molecule. The subscripts A and B are now used for acid and base.

$$\varphi_{A,p}^{v,s} = \varphi_{B,p}^{v,s} \tag{S.9}$$

$$s_{A,p}^{\perp}\, c_A^v\, \gamma_{A,p} = s_{B,p}^{\perp}\, c_B^v\, \gamma_{B,p} \tag{S.10}$$

$$\gamma_{B,p} = \frac{s_{A,p}^{\perp}\, c_A^v}{s_{B,p}^{\perp}\, c_B^v} \gamma_{A,p} \tag{S.11}$$

$$\gamma_{B,p} = r_{AB}^{v}\, \gamma_{A,p} \tag{S.12}$$

$$r_{AB}^{v} = \frac{s_{A,p}^{\perp}\, c_A^v}{s_{B,p}^{\perp}\, c_B^v} \tag{S.13}$$

In the case of base limiting experiments, $S_{B,p}$ is then found iteratively using the following equation, solved by combining Equations (S.7), (S.9) and (S.10). If the experiment is acid limiting, the difference in solving for $S_{A,p}$ is to replace r^v_{AB} with $1/r^v_{AB}$.

$$S_{B,p} = \frac{S_{AB,p}}{2}\left[\left(\frac{r^v_{AB}-1}{r^v_{AB}}\right) + \sqrt{\left(\frac{r^v_{AB}-1}{r^v_{AB}}\right)\frac{4}{r^v_{AB}S_{AB,p}}}\right] \quad \text{(S.14)}$$

Where $S_{AB,p}$ is the saturation of ammonium nitrate

$$S_{AB,p} = \frac{a^v_A a^v_B K^{eq}_{AB}}{K_{AB,p}} = \frac{x^v_A x^v_B}{K_{AB,p}K_p} \quad \text{(S.15)}$$

$$K_p = \frac{p^o_B p^o_A}{K^{eq}_{AB}} \quad \text{(S.16)}$$

Where x^v_A and x^v_B are the mixing ratios of nitric acid and ammonia respectively, K^{eq}_{AB} is the equilibrium constant for $NH_3(s) + HNO_3(s) \rightleftharpoons NH_4{\cdot}NO_3(s)$, K_p is an overall dissociation constant for ammonium nitrate condensation, i.e. $NH_3(v) + HNO_3(v) \rightleftharpoons NH_4{\cdot}NO_3(s)$, [25], and $K_{AB,p}$ is the Kelvin term for ammonium nitrate, correcting for the curvature effect of different sized particles.

$$K_{AB,p} = 10^{\left(d_{K10}/d_p\right)} \quad \text{(S.17)}$$

The Kelvin diameter for ammonium nitrate at 5 °C was calculated by fitting the data from CLOUD experiments (Figure S2) according to the relationship shown in Equation (S.18).

$$S_{AB,p} = 10^{\left(d_{K10}/d_{act}\right)} \quad \text{(S.18)}$$

Modelling nitric acid

In the two CLOUD experiments with high condensation sink (Figure 2), there were no accurate measurements of HNO_3 due to depleted reagent ions, and therefore the time-series presented are modelled concentrations. A box model was set up where HNO_3 was solved for based on sums of production and losses at each time step.

$$\frac{\partial HNO_3}{\partial t} = source_{injection} + source_{NO_2+\cdot OH} - loss_{wall+dilution} - loss_{condensation\ sink} \quad \text{(S.19)}$$

This model was tested on other CLOUD experiments and agreed with the measurements from the Br^- CI-API-TOF-MS within a factor of two.

OH was modelled in a similar way using the AtChem online solver where the chemical mechanistic information was taken from the Master Chemical Mechanism, MCM v3.3.1 [26,27]. Inputs were measured time series of various trace gases, photolysis rates of ozone and HONO, and chamber wall and dilution losses specific to CLOUD.

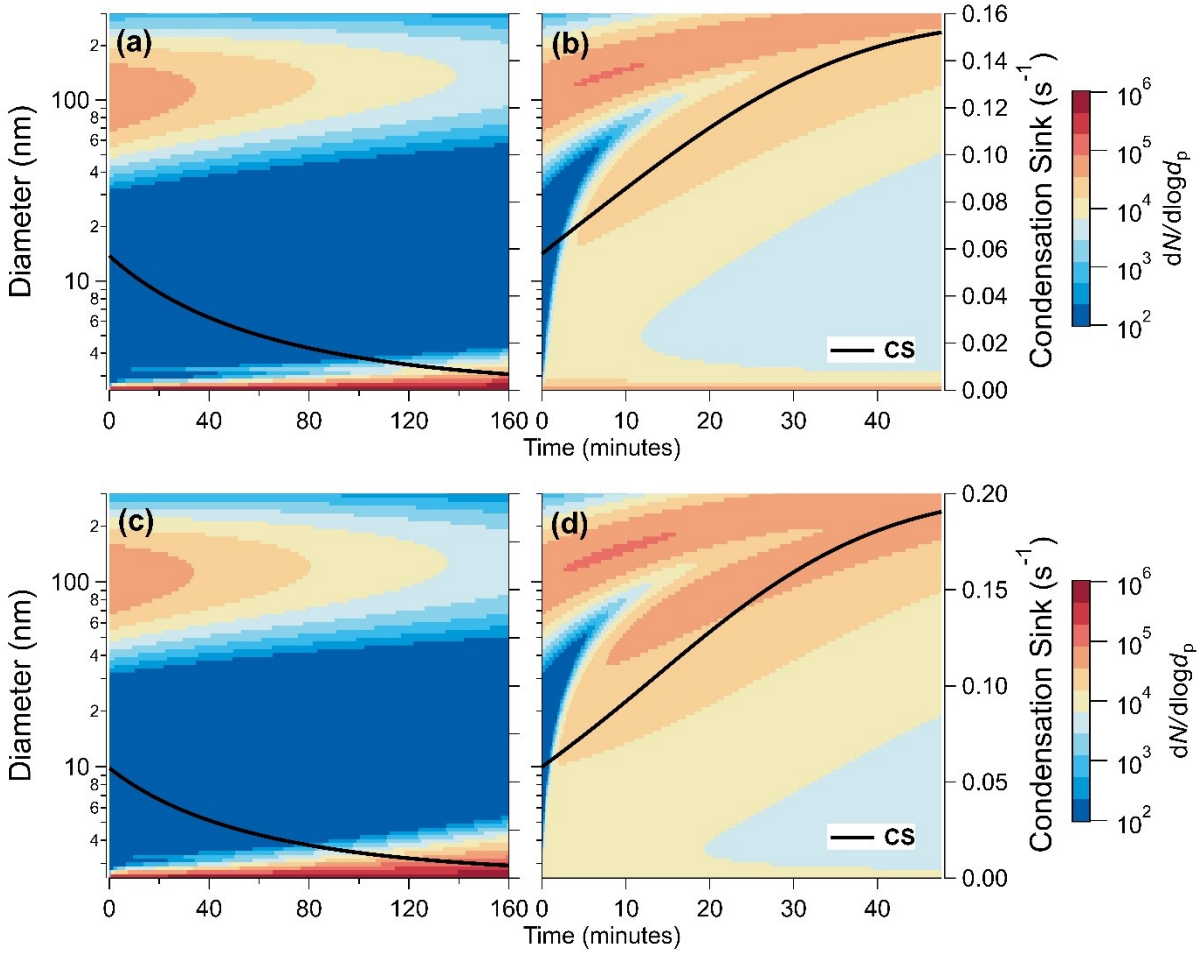

***Figure S1: Sensitivity tests on gas phase concentrations and formation rates on modelled results of Figure 2**: This figure is a repeat model of the runs in Figure 2 d and i of the main text but with **a-b)** $J_{2.5}$ constrained to 10 cm^3s^{-1}, and **c-d)** $J_{2.5}$ constrained to 10 cm^3s^{-1} as well as H_2SO_4 and NH_3 concentrations switched between the two experiments. All other experimental conditions are the same. The model results are similar to those in Figure 2 panels d and i, with little to no growth in the low HNO_3 case (a,c), and the "smear" of particles of all sizes in the high HNO_3 case (b, d).*

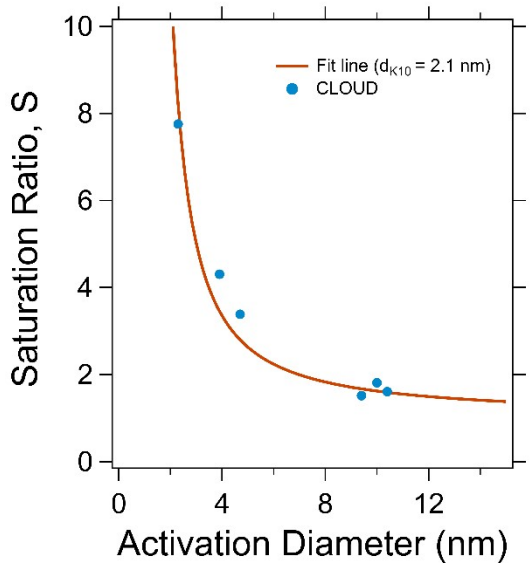

235

236 ***Figure S2: Saturation ratio vs activation diameter:*** *Blue markers represent measured activation diameters from CLOUD*
237 *experiments and saturation ratios calculated from measured HNO_3 and NH_3 gas phase concentrations. The red fit line is fit to*
238 *this data and then used to calculate the Kelvin diameter for use in the model.*

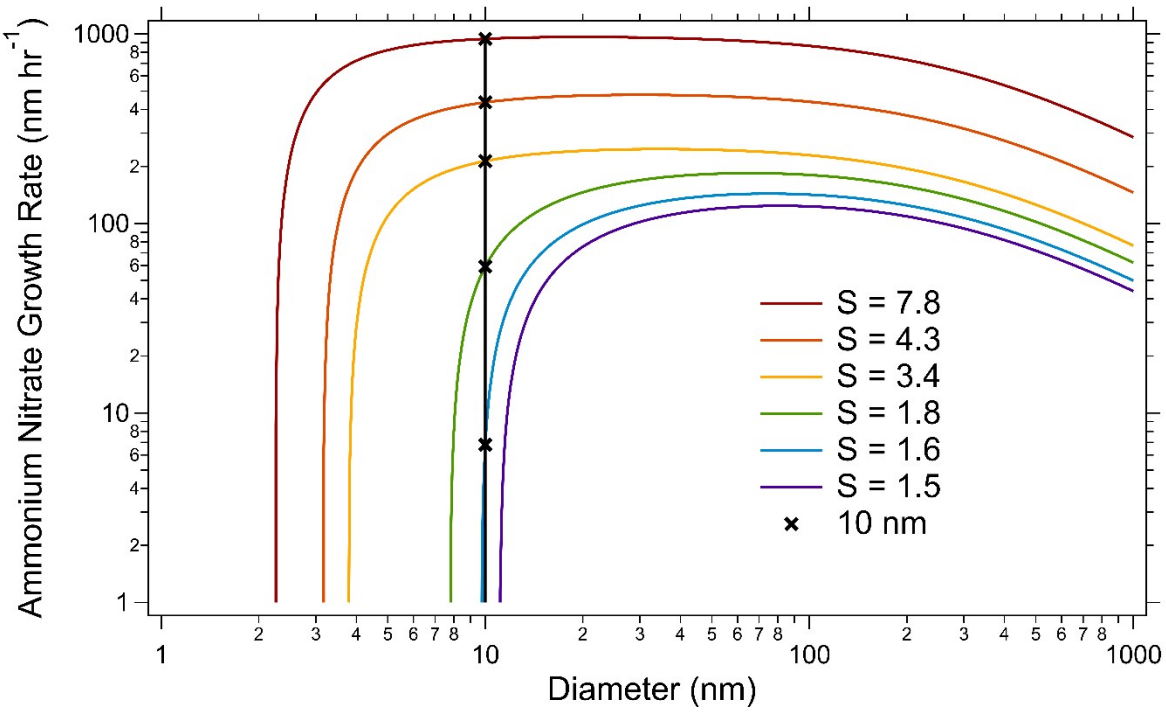

239

240 ***Figure S3: Diameter vs calculated growth rates from flux equations –*** *The curves are calculated using the equations in the*
241 *section "Modelling ammonium nitrate". The six S curves plotted are using S calculated from the HNO_3 and NH_3 gas*
242 *concentrations from the six CLOUD experiments shown in Figure 1. It is apparent that at low diameters the growth varies*
243 *dramatically, around the activation diameter for each S value.*

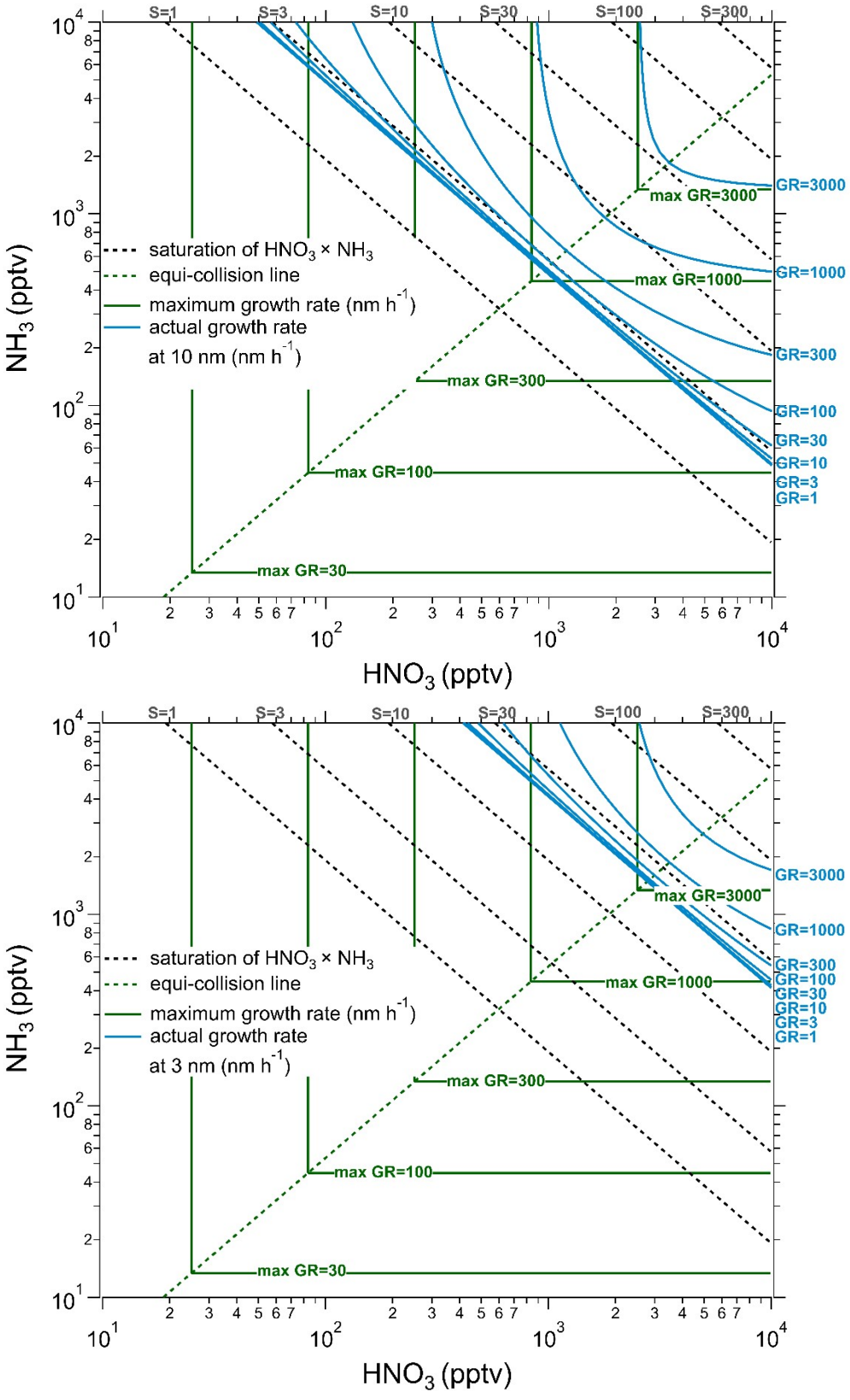

Figure S4: Calculated growth rates of condensation of ammonium nitrate: *The phase space shown is between 1 pptv and 10,000 pptv (10 ppbv) at 5 °C. The top panel shows growth rates for a particle of 10 nm and the bottom panel shows growth rates for a particle of 3 nm (the same size used for calculating growth rates in Figure 2) The calculations for growth rate include the Kelvin effect using the Kelvin diameter calculated (see modelling ammonium nitrate).*

References

1. Kirkby, J. *et al.* Role of sulphuric acid, ammonia and galactic cosmic rays in atmospheric aerosol nucleation. *Nature* **476**, 429–433 (2011).
2. Duplissy, J. *et al.* Effect of ions on sulfuric acid-water binary particle formation: 2. Experimental data and comparison with QC-normalized classical nucleation theory: BINARY PARTICLE FORMATION EXPERIMENTS. *J. Geophys. Res. Atmos.* **121**, 1752–1775 (2016).
3. Voigtländer, J., Duplissy, J., Rondo, L., Kürten, A. & Stratmann, F. Numerical simulations of mixing conditions and aerosol dynamics in the CERN CLOUD chamber. *Atmos. Chem. Phys.* **12**, 2205–2214 (2012).
4. Stolzenburg, D. *et al.* Enhanced growth rate of atmospheric particles from sulfuric acid. *Atmos. Chem. Phys.* **20**, 7359–7372 (2020).
5. Kürten, A., Rondo, L., Ehrhart, S. & Curtius, J. Performance of a corona ion source for measurement of sulfuric acid by chemical ionization mass spectrometry. *Atmos. Meas. Tech.* **4**, 437–443 (2011).
6. Tröstl, J. *et al.* The role of low-volatility organic compounds in initial particle growth in the atmosphere. *Nature* **533**, 527–531 (2016).
7. Kirkby, J. *et al.* Ion-induced nucleation of pure biogenic particles. *Nature* **533**, 521–526 (2016).
8. Canaval, E. *et al.* Rapid conversion of isoprene photooxidation products in terrestrial plants. *Commun Earth Environ* **1**, 44 (2020).
9. Breitenlechner, M. *et al.* PTR3: An Instrument for Studying the Lifecycle of Reactive Organic Carbon in the Atmosphere. *Anal. Chem.* **89**, 5824–5831 (2017).
10. Pfeifer, J. *et al.* Measurement of ammonia, amines and iodine species using protonated water cluster chemical ionization mass spectrometry. *Atmospheric Measurement Techniques Discussions* 1–36 (2019) doi:10.5194/amt-2019-215.
11. Vanhanen, J. *et al.* Particle Size Magnifier for Nano-CN Detection. *Aerosol Science and Technology* **45**, 533–542 (2011).

12. Stolzenburg, D., Steiner, G. & Winkler, P. M. A DMA-Train for precision measurement of sub-10nm aerosol dynamics. *Atmospheric Measurement Techniques* **10**, 1639–1651 (2017).
13. Kong, W. *et al.* The nano-scanning electrical mobility spectrometer (nSEMS) and its application to size distribution measurements of 1 . 5-25 nm particles. 1–26 (2021).
14. Cai, R. *et al.* Data inversion methods to determine sub-3 nm aerosol size distributions using the particle size magnifier. *Atmos. Meas. Tech.* **11**, 4477–4491 (2018).
15. Lehtipalo, K. *et al.* Methods for determining particle size distribution and growth rates between 1 and 3 nm using the Particle Size Magnifier. **19**, 22.
16. Tröstl, J. *et al.* Fast and precise measurement in the sub-20nm size range using a Scanning Mobility Particle Sizer. *Journal of Aerosol Science* **87**, 75–87 (2015).
17. Jurányi, Z. *et al.* A 17 month climatology of the cloud condensation nuclei number concentration at the high alpine site Jungfraujoch. *J. Geophys. Res.* **116**, D10204 (2011).
18. Wiedensohler, A. *et al.* Mobility particle size spectrometers: harmonization of technical standards and data structure to facilitate high quality long-term observations of atmospheric particle number size distributions. *Atmos. Meas. Tech.* **5**, 657–685 (2012).
19. Stolzenburg, D. *et al.* Rapid growth of organic aerosol nanoparticles over a wide tropospheric temperature range. *Proc Natl Acad Sci USA* **115**, 9122–9127 (2018).
20. Pichelstorfer, L. *et al.* Resolving nanoparticle growth mechanisms from size- and time-dependent growth rate analysis. *Atmos. Chem. Phys.* **18**, 1307–1323 (2018).
21. Ozon, M., Stolzenburg, D., Dada, L., Seppänen, A. & Lehtinen, K. E. J. Aerosol formation and growth rates from chamber experiments using Kalman smoothing. *Atmos. Chem. Phys.* **21**, 12595–12611 (2021).
22. Dada, L. *et al.* Formation and growth of sub-3-nm aerosol particles in experimental chambers. *Nat Protoc* **15**, 1013–1040 (2020).
23. Seinfeld, J., H. & Pandis, S., N. *Atmospheric Chemistry and Physics*. vol. 2nd edn (John Wiley & Sons, 2006).

24. Wang, M. *et al.* Rapid growth of new atmospheric particles by nitric acid and ammonia condensation. *Nature* **581**, 184–189 (2020).
25. Mozurkewich, M. The dissociation constant of ammonium nitrate and its dependence on temperature, relative humidity and particle size. *Atmospheric Environment. Part A. General Topics* **27**, 261–270 (1993).
26. Bloss, C. *et al.* Development of a detailed chemical mechanism (MCMv3.1) for the atmospheric oxidation of aromatic hydrocarbons. *Atmos. Chem. Phys.* 24 (2005).
27. Jenkin, M. E., Saunders, S. M., Wagner, V. & Pilling, M. J. Protocol for the development of the Master Chemical Mechanism, MCM v3 (Part B): tropospheric degradation of aromatic volatile organic compounds. *Part B* 13 (2003).